The vertical oscillations of coupled magnets

2011 Eur. J. Phys. 32 S1

(http://iopscience.iop.org/0143-0807/32/4/S01)

IOP PUBLISHING EUROPEAN JOURNAL OF PHYSICS

Eur. J. Phys. **32** (2011) S1–S14 doi:10.1088/0143-0807/32/4/S01

The vertical oscillations of coupled magnets

Li Kewei[1], Lin Jiahuang[1], Kang Zi Yang[1], Samuel Yee Wei Liang[2] and Jeremias Wong Say Juan[3]

[1] Raffles Institution, 1 Raffles Institution Lane, Singapore 575954
[2] Anglo-Chinese School Independent, 121 Dover Road, Singapore 139650
[3] NUS High School of Mathematics and Science, 20 Clementi Avenue 1, Singapore 129957

E-mail: likewei92@gmail.com

Received 4 January 2011, in final form 28 April 2011
Published 16 June 2011
Online at stacks.iop.org/EJP/32/S1

Abstract

The International Young Physicists' Tournament (IYPT) is a worldwide, annual competition for high school students. This paper is adapted from the winning solution to Problem 14, Magnetic Spring, as presented in the final round of the 23rd IYPT in Vienna, Austria. Two magnets were arranged on top of each other on a common axis. One was fixed, while the other could move vertically. Various parameters of interest were investigated, including the effective gravitational acceleration, the strength, size, mass and geometry of the magnets, and damping of the oscillations. Despite its simplicity, this setup yielded a number of interesting and unexpected relations. The first stage of the investigation was concerned only with the undamped oscillations of small amplitudes, and the period of small amplitude oscillations was found to be dependent only on the eighth root of important magnet properties such as its strength and mass. The second stage sought to investigate more general oscillations. A numerical model which took into account magnet size, magnet geometry and damping effects was developed to model the general oscillations. Air resistance and friction were found to be significant sources of damping, while eddy currents were negligible.

(Some figures in this article are in colour only in the electronic version)

1. Introduction

The International Young Physicists' Tournament (IYPT)[4] is a worldwide, annual competition for high school students. This paper is adapted from the winning solution to Problem 14, Magnetic Spring, as presented in the final round of the 23rd IYPT in Vienna, Austria.

[4] http://www.iypt.org.

Table 1. Magnet dimensions and masses.

Magnet	Type	Radius (cm)		Thickness (cm)	Mass (g)
		Inner	Outer		
A	Large ring	0.300	0.950	1.000	19.9
B	Large ring	0.300	0.950	1.000	19.8
C	Small button	–	0.600	0.600	7.3
D	Small button	–	0.600	0.600	7.3
E	Small ring	0.345	0.600	0.620	5.5
F	Small ring	0.345	0.600	0.620	5.5

When two magnets are arranged on top of each other such that one of them is fixed and the other one can move vertically, oscillatory motion may be observed. Despite the simplicity of the setup, our study revealed a few interesting relations. In typical oscillations, frequency increases with increased spring constant and decreases with increased inertia. In this setup, however, the frequency of small amplitude oscillations was found to decrease slowly as the strengths of the magnets were increased, and increase slowly as the mass of the oscillating magnet was increased. To gain physical insight into how these seemingly paradoxical relations arose, undamped oscillations with small amplitudes were first studied. A more general model accounting for damping due to air resistance and friction, the finite size and geometry of the magnets as well as large amplitude oscillations is formulated in the second part of the paper.

Similar studies on oscillations involving magnets have been conducted before, but this particular motion has not been fully investigated. Heddle (1970) reported that ring magnets are suitable as a demonstration of strongly coupled oscillators, but did not conduct a detailed investigation. Haines and Michaelis (1989) carried out a detailed experimental and theoretical study on magnets suspended by Pierrus suspension, but left out vertical oscillations. Geim *et al* (1999) focused on the levitation of magnets using diamagnetic materials without investigation of oscillations. More recently, Moloney (2008) conducted an investigation on coupled oscillations of two magnets placed at the same height.

2. Materials

Cylindrical neodymium magnets were used in all our experiments. Three types of magnets were used: large ring magnets, small button magnets and small ring magnets. The masses of the magnets were found using a digital mass balance, and the dimensions of the magnets were measured with vernier calipers. Table 1 shows the dimensions and mass of each magnet.

3. Oscillations with small amplitudes

The first experiments were conducted to investigate undamped small amplitude oscillations. To minimize damping, the experiments were conducted on an air track, as shown in figure 1. The mass of an air track cart was found using an electronic weighing balance to be 183.0 g. The air track was supported by a lab jack on one end; by varying the height of the jack, the angle of tilt of the track was varied. The angle of tilt determines the value of effective gravitational acceleration, which is an independent variable in the experiment.

The magnets were made to settle in their equilibrium positions before the oscillating magnet was displaced about 0.5 cm from equilibrium and allowed to oscillate. The time

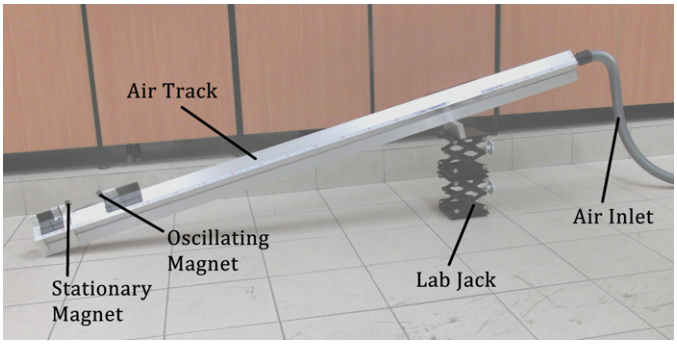

Figure 1. Experimental setup used to investigate small amplitude oscillations.

taken for 40 oscillations was recorded and used to determine the oscillation frequency. This procedure was repeated for each angle of tilt and type of magnet.

A theoretical model which produces key features of the oscillations was formulated. For simplicity, the magnets were assumed to be uniformly magnetized with their magnetization parallel to the axis of symmetry of the cylinder. Because the magnets are small compared to the distance between them (about 6 cm), they may be treated as point dipoles with dipole moments of magnitude μ_{M_1} and μ_{M_2}. Point dipoles serve as good approximations for button magnets due to their simple geometry. The ring magnet is more complicated due to its central cavity, but its magnetic field still approximates that of a dipole at large distances, as shown in figure 2. The magnetic field, $\mathbf{B}$, generated by the stationary magnet with dipole moment μ_{M_1} is (Griffiths 1999)

$$\mathbf{B} = \frac{\mu_0 \mu_{M_1}}{4\pi r^3}(2\cos\theta\hat{\mathbf{r}} + \sin\theta\hat{\boldsymbol{\theta}}) \tag{1}$$

where $\hat{\mathbf{r}}$ and $\hat{\boldsymbol{\theta}}$ are given in figure 3. In our investigation, the magnets are oscillating along the z axis; thus, θ is 0.

The magnetic energy associated with the interaction between μ_{M_1} and μ_{M_2} is given by (Griffiths 1999)

$$U = -\boldsymbol{\mu}_{M_2} \cdot \mathbf{B}. \tag{2}$$

μ_{M_1} and μ_{M_2} were obtained from an experimental plot of $\mathbf{B}$ against z, as measured by a Hall probe. A plot of potential energy against the separation between the magnets is shown in figure 4. The minimum in the potential energy graph is the equilibrium position of the oscillations. The dipole model indicates that increases in potential energy on both sides of the equilibrium position are asymmetrical. Thus, the resulting oscillations will, in general, be nonlinear, something which we will consider in detail when formulating the general model in section 4. The force F_M on the magnet can then be found by taking the slope of the energy function:

$$F_M = -\frac{\mathrm{d}U}{\mathrm{d}z} = \mu_{M_2}\frac{\mathrm{d}B}{\mathrm{d}z}. \tag{3}$$

Substituting equation (1) into equation (3) gives the equation of motion for this oscillation:

$$m\ddot{z} = \frac{3\mu_0 \mu_{M_1}\mu_{M_2}}{2\pi z^4} - mg. \tag{4}$$

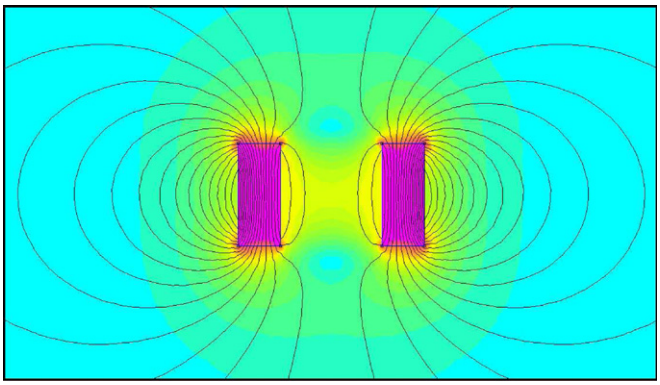

(a)

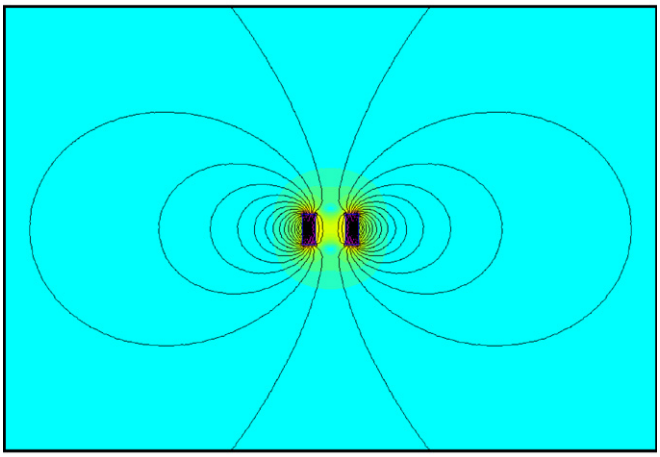

(b)

Figure 2. The field around a ring magnet. (a) At small distances. (b) At large distances, the field approximates that of a dipole.

At the equilibrium position, the force is zero. Thus, the equilibrium position z_0 is given by

$$z_0 = \sqrt[4]{\frac{3\mu_0\mu_{M_1}\mu_{M_2}}{2\pi mg}}. \tag{5}$$

Let $x = z - z_0$ be the displacement from equilibrium. Binomial expansion to the first order can be used to approximate the expression of the magnetic force for small displacements from equilibrium:

$$m\ddot{x} \approx -\frac{6\mu_0\mu_{M_1}\mu_{M_2}}{\pi z_0^5}x. \tag{6}$$

Under this first-order approximation, the oscillations become simple harmonic with frequency f, given by

$$f = \left(\frac{2m}{3\pi^7\mu_0\mu_{M_1}\mu_{M_2}}\right)^{\frac{1}{8}} g^{\frac{5}{8}} \tag{7}$$

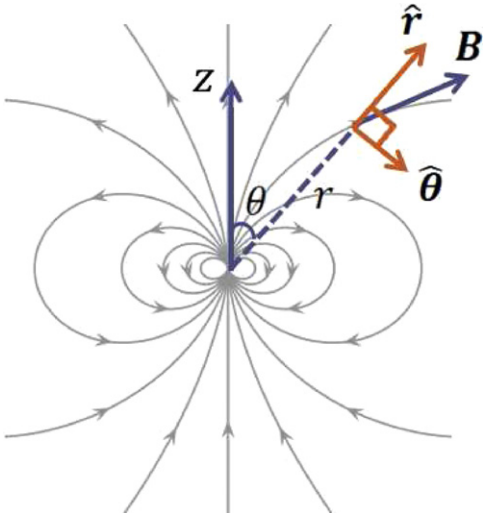

Figure 3. Definition of coordinates in equation (1).

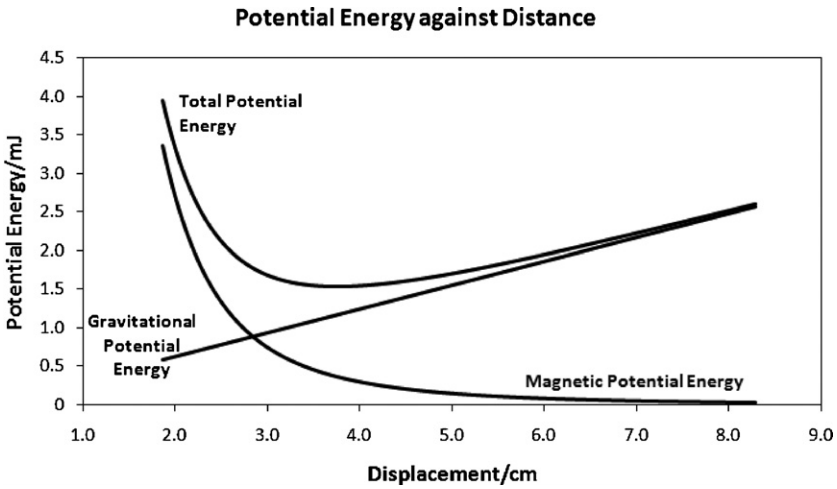

Figure 4. Potential energy against displacement for magnets E and F.

where m is the combined mass of the oscillating magnet plus the air track cart and g is the value of effective gravitational acceleration. This equation grants much physical insight into the oscillations.

First, the frequency of the oscillations increases very gradually with the eighth root of mass. This may initially seem counter-intuitive, as the frequency normally decreases with increasing inertia. However, besides causing an increase in inertia, the increased mass of the magnet also brings the equilibrium position closer to the fixed magnet, where the axial magnetic field varies much more rapidly with respect to z. This produces an increase in the spring constant, thus increasing the frequency of the oscillations. In this case, the addition of mass brings out two competing effects, one of which dominates slightly, explaining why the frequency depends only on the eighth root of mass.

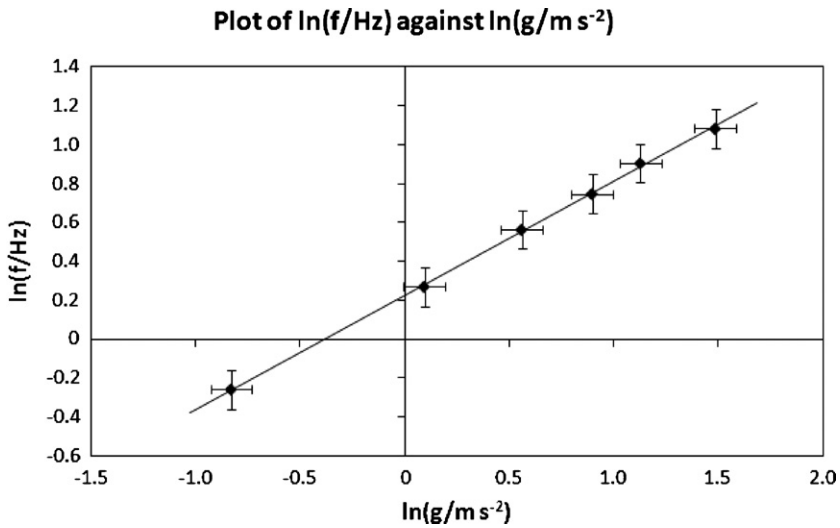

Figure 5. Graph of results obtained for the oscillation of large ring magnets A and B.

Table 2. Summary of results for small amplitude oscillations.

Fixed magnet	Oscillating magnet	Experimental slope	% deviation from theory
C (small button)	D (small button)	0.600	4.0
C (small button)	B (large ring)	0.597	4.5
E (small ring)	D (small button)	0.592	5.3
A (large ring)	B (large ring)	0.587	6.1
E (small ring)	F (small ring)	0.585	6.4
A (large ring)	F (small ring)	0.583	6.7

Secondly, the frequency of the oscillations decreases as the magnetic moments of the magnets are increased. This may seem counter-intuitive again, as a greater magnetic moment should result in a greater spring constant and thus an increase in frequency instead. The resolution again lies in the change in equilibrium position. An increase in magnetic moment pushes the equilibrium position further from the fixed magnet, resulting in a decrease in the spring constant. Again there are two competing factors, explaining why the frequency is also only dependent on the eighth root of the magnetic moments.

Thirdly, the frequency is directly proportional to the $5/8$th power of the effective gravitational acceleration. Thus, a plot of ln(frequency/Hz) against ln(effective gravitational acceleration/m s^{-2}) should produce a straight line with the slope of $5/8 = 0.625$. Experimental data were plotted this way and figure 5 shows a graph of the data that were obtained for the oscillation of large ring magnets. Other experiments with magnets of different sizes and geometries gave similar graphs.

The data obtained do indeed give a straight line, as predicted by theory. The experimental slope can be compared to the theoretical value of 0.625, and table 2 summarizes the results of this comparison for various magnet sizes and geometries. The data were arranged in ascending order of deviation from the theoretical slope of 0.625.

Small button magnets followed theoretical predictions the most closely, because their small size and simple geometry make the point dipole an excellent approximation. Whenever large magnets or ring magnets were used, the deviations from theoretical predictions were more significant. This is expected because the dipole approximation becomes less accurate.

The investigation into small amplitude oscillations has allowed us to gain valuable physical insight. However, the data indicate that the dipole approximation begins to fail whenever large magnets or ring magnets were used. The investigation also did not consider the effects of large amplitude oscillations and damping.

4. General oscillations

Moving away from the simplifying assumptions in the previous section, a more general investigation into oscillations with large amplitudes, complicated magnet geometries and damping was conducted.

Since this investigation focuses on the geometry of the magnets and damping, another experimental setup was used. The two small ring magnets E and F were threaded on a glass rod attached to a wooden base. Magnet E was fixed at the bottom of the rod. A high-speed digital camera was positioned in front of the setup, as shown in figure 6.

The slight difference between the inner diameter of the ring magnet and the diameter of the glass rod results in the magnet slanting. The slanting of the magnet is a non-ideal part of the setup that does not add any value to our investigation; thus, it was minimized through the addition of a straw. The straw also reduced contact friction, allowing more oscillations to be observed. When the magnet and straw slant, the top of the straw comes into contact with the glass rod first. To prevent further slanting, the contact force with the glass rod must exert an equal and opposite torque to the torque experienced by magnet F. The long straw increases the moment arm of the contact force, thus reducing the force required for the same torque. Since friction is proportional to the normal contact force, the contact friction is reduced too.

The suspended magnet was released from five different initial displacements at 5.0 cm intervals, and a high-speed camera was used to record its motion at 600 frames s^{-1}. Frame-by-frame video analysis was performed to obtain an experimental graph of displacement against time. A representative example of a graph obtained is shown in figure 7. Other graphs with different initial displacements showed similar trends.

A general model that considers the geometry of the magnets and damping effects was formulated. In classical electrodynamics, permanent magnetism can be represented as equivalent currents (Griffiths 1999), as shown in figure 8. In uniformly magnetized cylindrical magnets, all magnetic properties can be modelled with surface currents on the curved surfaces. In the case of a ring magnet where two curved surfaces are present, the inner and outer surfaces have currents of equal magnitude flowing in opposite directions.

The surface current density, $\mathbf{K_s}$, is given by

$$\mathbf{K_s} = \mathbf{M} \times \hat{\mathbf{n}} \tag{8}$$

where $\hat{\mathbf{n}}$ is the area unit vector of the magnet surface (which points radially outwards on the outer magnet surface, and radially inwards on the inner magnet surface) and $\mathbf{M}$ is the magnetization of the magnet, defined as the magnetic moment per unit volume.

We derived the force arising from the magnetic field of a fixed cylindrical current sheet acting on another suspended current sheet, in the arrangement shown in figures 9(a) and (b). Subscript 1 denotes the properties of the fixed current sheet, while subscript 2 denotes the properties of the suspended current sheet.

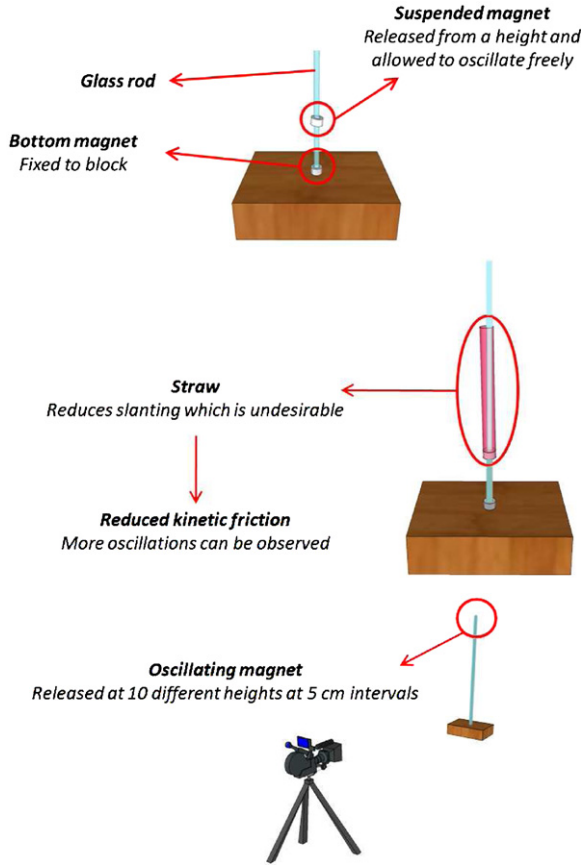

Figure 6. Experimental setup for the general investigation.

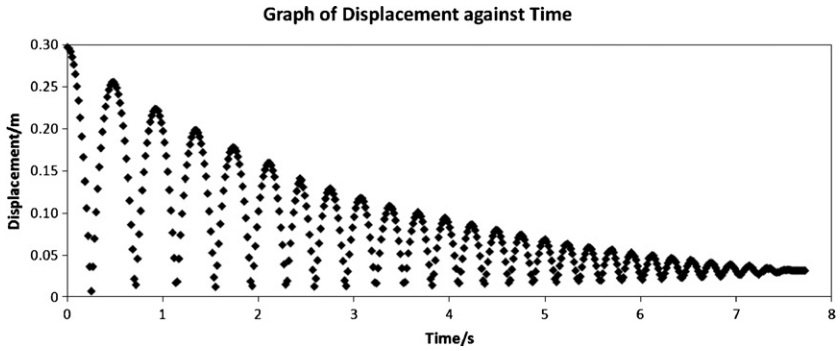

Figure 7. Experimental displacement against time graph of magnet F dropped from an initial displacement of 30.0 cm.

The magnetic field generated by the bottom current sheet at the field point, shown in figure 9(b), must first be found using the Biot–Savart law:

$$\mathbf{B} = \frac{\mu_0}{4\pi} \int \frac{i_1 \, \mathrm{d}\mathbf{l} \times \mathbf{r}}{r^3} \tag{9}$$

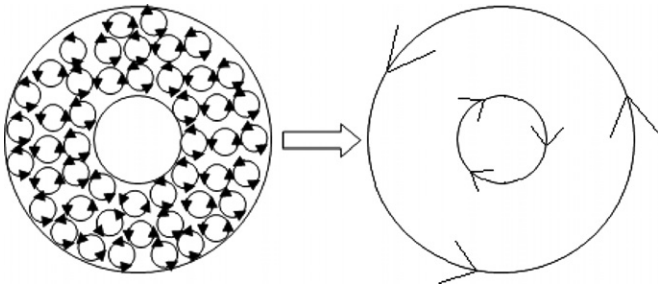

Figure 8. Uniformly magnetized permanent magnets and their equivalent representation using surface currents.

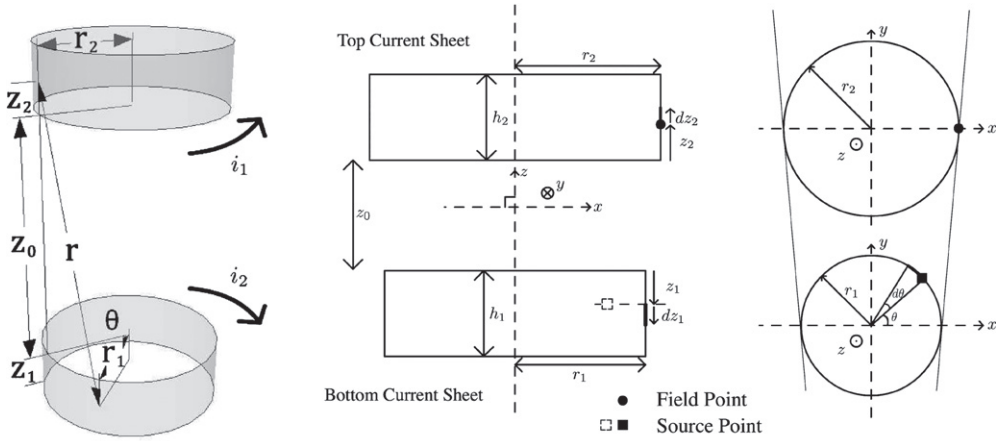

Figure 9. The model for two cylindrical current sheets.

where

$$i_1 = |\mathbf{K_{s_1}}|\mathrm{d}z_1 = |\mathbf{M_1}|\mathrm{d}z_1 \tag{10}$$

is the infinitesimal current flowing in a ring element of height dz.

From figure 9(a), the geometry of the system gives

$$\mathrm{d}\mathbf{l} = r_1\,\mathrm{d}\theta \begin{pmatrix} -\sin\theta \\ \cos\theta \\ 0 \end{pmatrix}, \tag{11}$$

$$\mathbf{r} = \begin{pmatrix} r_2 - r_1\cos\theta \\ -r_1\sin\theta \\ z_0 + z_1 + z_2 \end{pmatrix} \tag{12}$$

and

$$|\mathbf{r}| = \sqrt{(r_2 - r_1\cos\theta)^2 + (-r_1\sin\theta)^2 + (z_0 + z_1 + z_2)^2}. \tag{13}$$

Thus,

$$\mathrm{d}\mathbf{l} \times \mathbf{r} = r_1 \,\mathrm{d}\theta \begin{pmatrix} (z_0 + z_1 + z_2)\cos\theta \\ (z_0 + z_1 + z_2)\sin\theta \\ r_1 - r_2\cos\theta \end{pmatrix}. \tag{14}$$

Substituting equations (13) and (14) into the Biot–Savart law gives

$$B_x = \frac{\mu_0}{4\pi} \int \frac{i_1 r_1 (z_0 + z_1 + z_2)\cos\theta}{r^3}\,\mathrm{d}\theta. \tag{15}$$

This integral, however, only gives the magnetic field due to an infinitesimal surface current i_1 flowing in a ring element. To obtain the total magnetic field produced by the current sheet, another integration has to be performed over the height of the magnet. At the field point, we let the x axis be in the radial direction and the y axis be in the tangential direction. From the symmetry of the system, $B_y = 0$. The radial component of the magnetic field is thus

$$\begin{aligned} B_r &= B_x \\ &= \frac{\mu_0}{4\pi} \int_{-\pi}^{\pi} \int_0^h |\mathbf{M_1}| \frac{r_1 (z_0 + z_1 + z_2)\cos\theta}{[(r_2 - r_1\cos\theta)^2 + (-r_1\sin\theta)^2 + z^2]^{\frac{3}{2}}}\,\mathrm{d}z_1\,\mathrm{d}\theta \end{aligned} \tag{16}$$

where h is the height of the magnet.

Having obtained an expression for the magnetic field, the force acting on the suspended current sheet can be calculated using the Lorentz force:

$$\mathbf{F} = i\mathbf{l} \times \mathbf{B} \tag{17}$$

where $\mathbf{F}$ is the magnetic force, i is the current in the conductor, $\mathbf{l}$ is the length vector in the direction of the current and $\mathbf{B}$ is the magnetic field through the length. Hence, the total magnetic force, F_{Magnetic}, is

$$\begin{aligned} F_{\text{Magnetic}} &= \int_0^h |\mathbf{M_2}|\,\mathrm{d}z_2 \cdot 2\pi r_2 \cdot B_r \\ &= \frac{\mu_0}{4\pi} \int_{-\pi}^{\pi} \int_0^h \int_0^h |\mathbf{M_1}||\mathbf{M_2}| \frac{r_1 (z_0 + z_1 + z_2)\cos\theta \quad \mathrm{d}z_1\,\mathrm{d}z_2\,\mathrm{d}\theta}{[(r_2 - r_1\cos\theta)^2 + (-r_1\sin\theta)^2 + z^2]^{\frac{3}{2}}}. \end{aligned} \tag{18}$$

If the magnitudes of the magnetizations $|\mathbf{M_1}|$ and $|\mathbf{M_2}|$ are known, numerical integration can be performed to evaluate the force between the two current sheets. The interaction between ring magnets was modelled as the interaction between four current sheets.

To measure the magnetization of the magnets, a graph of magnetic field strength against the distance from the magnet was obtained experimentally and compared with theory. The axial magnetic field due to a ring magnet is (Pollack and Stump 2002)

$$B_z(z) = \frac{\mu_0 |\mathbf{M}|}{2} \left(\frac{h - z}{\sqrt{a_1^2 + (h - z)^2}} + \frac{z}{\sqrt{a_1^2 + z^2}} \quad - \frac{h - z}{\sqrt{a_2^2 + (h - z)^2}} - \frac{z}{\sqrt{a_2^2 + z^2}} \right) \tag{19}$$

where B_z is the axial magnetic field strength, μ_0 is the permeability of free space, $|\mathbf{M}|$ is the magnitude of the magnetization, h is the magnet height, z is vertical distance from the bottom of the magnet, and a_1 and a_2 are the radii of the inner and outer current sheets, respectively.

A Hall probe (Pasco Hall Probe, model CI-6520, maximum field 0.2 T) connected to a data logger was used to measure the axial field of a ring magnet at different displacements, every 1 mm along the axis. To align the axis of the Hall probe with the axis of the ring magnet, both the Hall probe and the ring magnet were inserted into a single plastic straw that is of the same diameter as the Hall probe and the magnet. An experimental graph of magnetic field against displacement was obtained, as shown in figure 10.

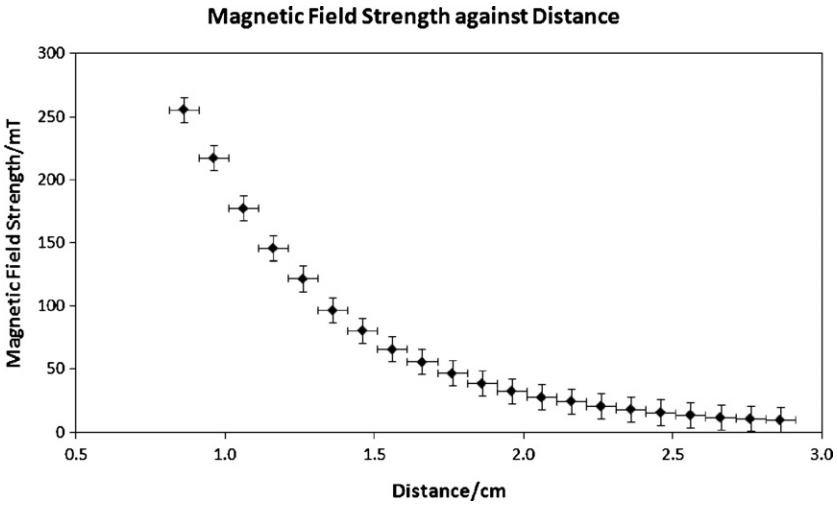

Figure 10. Experimental graph of axial magnetic field strength against distance for magnet E.

Table 3. Magnetization of the magnets.

Magnet	Type	Inner radius (cm)	Outer radius (cm)	Thickness (cm)	Mass (g)	Magnetization (kA m^{-1})
E	Small ring	0.600	0.345	0.620	5.5	1010
F	Small ring	0.600	0.345	0.620	5.5	1089

This graph was compared to equation (19) to determine values of magnetization through curve fitting. Table 3 shows the magnetization of the magnets. With the magnetizations known, the force between the magnets can be calculated by numerically integrating equation (18).

As a consistency check, the force between the two magnets was characterized experimentally and compared with theoretical values calculated from numerical integration. Weights of known masses were loaded onto the magnet and the distance between the magnets measured. The comparison between the theoretical and experimental values is shown in figure 11.

The magnetic force predicted by the general model agrees well with experimental values. This ensures that the model is accurate. Apart from the restoring forces of magnetism and gravity, damping due to air resistance and friction must also be taken into account. The effects of eddy currents were neglected. This will be justified in the next section. The air resistance, $-k_1\dot{\mathbf{z}}$, was taken to be proportional to the velocity, while the friction, $-k_2\hat{\dot{\mathbf{z}}}$, was taken to be a constant force acting in the opposite direction to velocity. Hence, the final equation of motion is

$$m\ddot{\mathbf{z}} = \mathbf{F}_{\text{Magnetic}} - m\mathbf{g} - k_1\dot{\mathbf{z}} - k_2\hat{\dot{\mathbf{z}}} \tag{20}$$

where k_1 is the air drag coefficient, k_2 is the magnitude of the average contact friction acting on the oscillating magnet and $\hat{\dot{\mathbf{z}}}$ is the sign of the velocity. Given the initial conditions, this equation can be numerically solved to obtain the theoretical displacement against time graph. The theoretical graph alongside the experimental data is shown in figure 12.

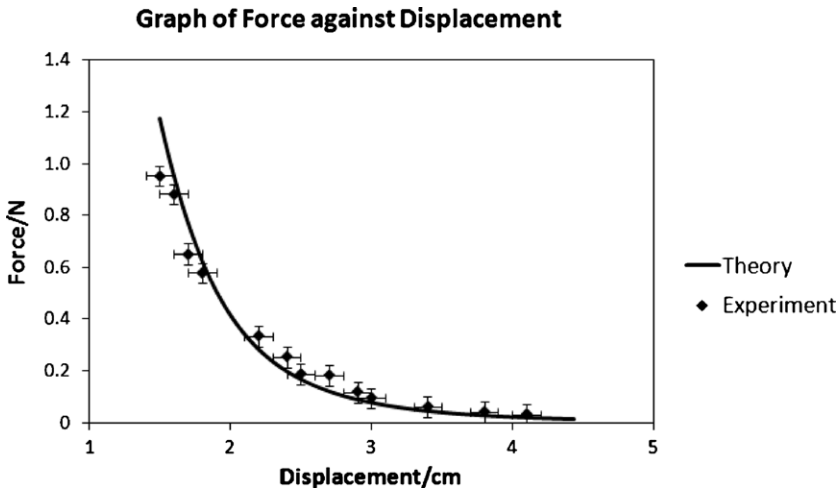

Figure 11. Comparison of experimental magnetic force between magnets E and F against displacement with theoretical values.

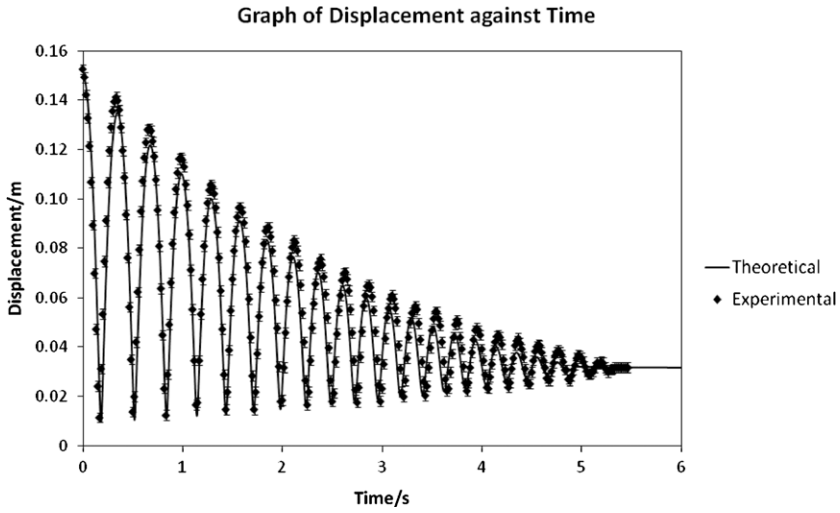

Figure 12. Comparison of experimental displacement against time graph with theoretical predictions for magnet F dropped from 15.0 cm.

A prominent feature of the oscillations is that they are nonlinear at large amplitudes. The magnetic force changes much more rapidly as the magnets get closer than the equilibrium displacement, giving rise to the nonlinearity of the oscillations.

The oscillations are clearly damped over time. The constants k_1 and k_2 were determined by optimizing the resultant curves with the experimental data across all experimental runs. k_1 was found to be 2×10^{-3} N s m^{-1}, while k_2 was found to be 3×10^{-4} N. These values are physically reasonable when compared to the magnet weight of 5.5×10^{-2} N, since experimental data suggest that the damping forces are small compared to the magnet weight, but still have a significant impact after a few oscillations. The envelope of damping is neither exponential (as

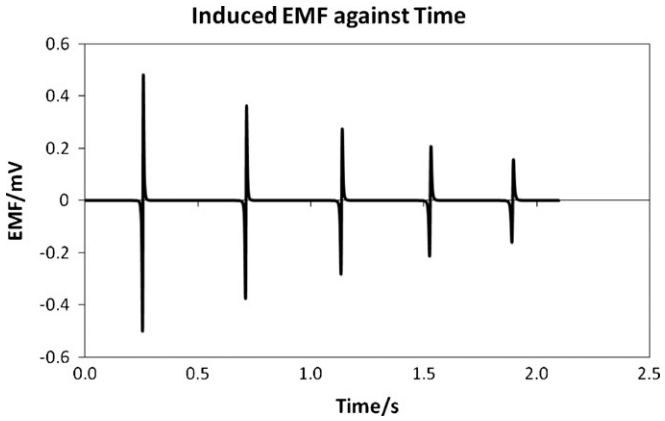

Figure 13. Graph of induced EMF against time for magnet F dropped from 30.0 cm.

would be expected if only air resistance were present) nor linear (as would be expected if only friction were present). This shows that air resistance and friction are approximately the same order of magnitude, in agreement with the optimized values.

Generally, a good fit between theory and data was observed during the first few oscillations of the magnet. However, as the oscillations continue, the theoretical predictions begin to deviate from experimental data. Comparing across the different experimental runs, this deviation appears to be random. The theoretical predictions did not produce consistently higher/lower amplitudes or longer/shorter periods. Thus, the deviations are probably due to chaotic factors in the setup. A possible source of chaos is the wobbling of the magnet due to the imperfect fit between the ring magnet and its guide. This can affect the contact friction, resulting in unpredictable variations from the constant force used to formulate the model. Given a long time over which to act, these effects caused the deviations seen in later oscillations. Such effects are non-deterministic and cannot be easily accounted for theoretically.

5. Effects of eddy currents

Here we justify our earlier claim that eddy currents are negligible. Eddy currents are generated by a changing magnetic flux. The induced EMF can be calculated from Faraday's law:

$$|\varepsilon| = \frac{\mathrm{d}\Phi_B}{\mathrm{d}t} = A\frac{\mathrm{d}B}{\mathrm{d}z}\frac{\mathrm{d}z}{\mathrm{d}t} = \pi a_1^2\frac{\mathrm{d}B}{\mathrm{d}z}\frac{\mathrm{d}z}{\mathrm{d}t} \tag{21}$$

where Φ_B is the magnetic flux through the oscillating magnet, A is the area of the oscillating magnet and a_1 is the outer radius of the oscillating magnet. The graph of induced EMF against time can be evaluated for the oscillation started at 30.0 cm, where the effects of eddy currents are expected to be the greatest. The graph produced is shown in figure 13.

Figure 13 shows that the maximum magnitude of the induced EMF is of the order of 40 mV. The resistance, R, of the magnet was measured to be 1.2 Ω through the use of a Soundtech Electronic EM390 multimeter. From this, the energy dissipated due to the eddy current can be approximated as

$$E_{\text{dissipated}} \approx \frac{\varepsilon^2}{R}\Delta t \tag{22}$$

where Δt is the width of the peak shown in figure 13. From figure 13, it is observed that the induced EMF comes in sharp peaks and provides a physical justification for these estimations. These sharp peaks allow us to estimate the energy dissipation from the peaks alone, while safely neglecting the induced EMF for other parts of the motion. Carrying out the calculations, the energy dissipated in the highest pair of peaks is about 3 nJ, roughly 0.1% of the energy of the slowest moving magnet. This should not be surprising given the low velocity of the magnet and its relatively high resistance. Thus, it can be safely concluded that eddy currents do not have a significant impact on the oscillations.

6. Conclusion

The vertical oscillations of coupled magnets yield a number of interesting relations despite their simplicity. We first studied small amplitude oscillations, and found that the oscillation frequency varies only with the eighth root of magnet properties such as their magnetization and mass. Deviations from the formulated model were attributed to the geometry of the magnets. Using numerical methods, a more general investigation took into account the geometry of the magnets, oscillations of large amplitudes and damping effects. The theoretical predictions from the general model fitted well with experimental observations within experimental error.

Acknowledgments

We would like to thank Dr Yeo Ye (National University of Singapore), Mrs Theresa Lai, Mr Mark Wee and Dr Tan Guoxian (Raffles Institution, Singapore), Mr Daniel Lo Yiu Wah and Mr Gao Guangyan for their tremendous help and support during our experiments and for the IYPT.

References

Geim A, Simon M, Boamfa M and Heflinger L 1999 *Nature* **400** 323–4
Griffiths D J 1999 *Introduction to Electrodynamics* (Englewood Cliffs, NJ: Prentice-Hall)
Haines C and Michaelis M 1989 *Phys. Educ.* **24** 359–64
Heddle D W O 1970 *Phys. Educ.* **5** 244–5
Moloney M J 2008 *Am. J. Phys.* **76** 125–8
Pollack G L and Stump D R 2002 *Electromagnetism* (Reading, MA: Addison-Wesley)